PROCEEDINGS OF SPIE

SPIEDigitalLibrary.org/conference-proceedings-of-spie

Imaging cellular and subcellular structure of human brain tissue using micro computed tomography

Anna Khimchenko
Christos Bikis
Gabriel Schweighauser
Jürgen Hench
Alexandra-Teodora Joita-Pacureanu
Peter Thalmann
Hans Deyhle
Bekim Osmani
Natalia Chicherova
Simone E. Hieber
Peter Cloetens
Magdalena Müller-Gerbl
Georg Schulz
Bert Müller

SPIE.

Invited Paper

Imaging cellular and subcellular structure of human brain tissue using micro computed tomography

Anna Khimchenko[a*], Christos Bikis[a], Gabriel Schweighauser[b], Jürgen Hench[b], Alexandra-Teodora Joita-Pacureanu[c], Peter Thalmann[a], Hans Deyhle[a], Bekim Osmani[a], Natalia Chicherova[a], Simone E. Hieber[a], Peter Cloetens[c], Magdalena Müller-Gerbl[d], Georg Schulz[a], and Bert Müller[a]

[a] Biomaterials Science Center, Department of Biomedical Engineering, University of Basel, Gewerbestrasse 14, 4123 Allschwil, Switzerland;
[b] Institute of Pathology, Department of Neuropathology, Basel University Hospital, Schönbeinstrasse 40, 4056 Basel, Switzerland;
[c] ID16A-NI Nano-Imaging Beamline, European Synchrotron Radiation Facility, 38043 Grenoble, France;
[d] Musculoskeletal Research Group, Department of Biomedicine, University of Basel, Pestalozzistrasse 20, 4056 Basel, Switzerland

ABSTRACT

Brain tissues have been an attractive subject for investigations in neuropathology, neuroscience, and neurobiology. Nevertheless, existing imaging methodologies have intrinsic limitations in three-dimensional (3D) label-free visualisation of extended tissue samples down to (sub)cellular level. For a long time, these morphological features were visualised by electron or light microscopies. In addition to being time-consuming, microscopic investigation includes specimen fixation, embedding, sectioning, staining, and imaging with the associated artefacts. Moreover, optical microscopy remains hampered by a fundamental limit in the spatial resolution that is imposed by the diffraction of visible light wavefront. In contrast, various tomography approaches do not require a complex specimen preparation and can now reach a true (sub)cellular resolution. Even laboratory-based micro computed tomography in the absorption-contrast mode of formalin-fixed paraffin-embedded (FFPE) human cerebellum yields an image contrast comparable to conventional histological sections. Data of a superior image quality was obtained by means of synchrotron radiation-based single-distance X-ray phase-contrast tomography enabling the visualisation of non-stained Purkinje cells down to the subcellular level and automated cell counting. The question arises, whether the data quality of the hard X-ray tomography can be superior to optical microscopy. Herein, we discuss the label-free investigation of the human brain ultramorphology be means of synchrotron radiation-based hard X-ray magnified phase-contrast in-line tomography at the nano-imaging beamline ID16A (ESRF, Grenoble, France). As an example, we present images of FFPE human cerebellum block. Hard X-ray tomography can provide detailed information on human tissues in health and disease, improving understanding of the neuro-degenerative diseases.

Keywords: Micro computed tomography, phase contrast, brain tissue, cerebellum, Purkinje cell, holotomography, single-distance tomography, in-line tomography, propagation-based imaging, virtual histology.

1. INTRODUCTION

The brain, having a multi-scale organisation, is one of the most complex organs within the body.[1] The human brain is much more complex than brains of rodents or invertebrates.[2] The mechanisms involved in brain functioning and de-/re-generation are not entirely understood. The rate of brain disorders is continuously increasing.[3] In the medical field, morphology – structure is strongly correlated with physiology – functioning. Thus, to understand brain's properties and functionality at the most fundamental level, data about the three-dimensional

* anna.khimchenko@unibas.ch; phone: +41 61 207 54 41; fax: +41 61 207 54 99; bmc.unibas.ch

Developments in X-Ray Tomography XI, edited by Bert Müller, Ge Wang, Proc. of SPIE Vol. 10391, 103910K · © 2017 SPIE · CCC code: 0277-786X/17/$18 · doi: 10.1117/12.2274120

(3D) architecture and organisation is essential, in particular with a higher precision level than provided, e.g., by magnetic resonance imaging (MRI). Thus, the brain remains an attractive subject for investigating the neuropathology[4,5] in the framework of correlating brain ultrastructure to its (dys)function.

The basic structural and functional unit of humans is the cell, highlighting the importance of investigations down to this level. In general, the visualisation and related analysis of neural tissue remains challenging.[6] Comprehensive understanding of the brain's functions and thereby diagnosis and treatment of its disorders, is hindered by the inability of currently available imaging techniques to provide with an isotropic (sub)cellular resolution in a label-free and non-destructive manner for tissue specimens large enough to represent sufficient volumes for investigation, see Figure 1.

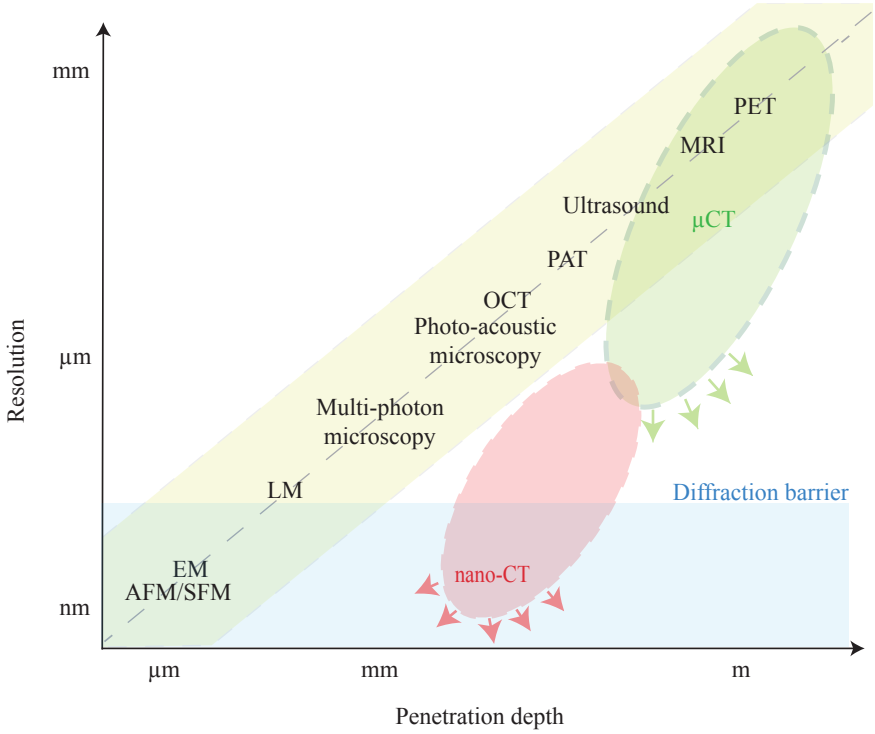

Figure 1. Spatial resolution versus penetration depth for some of the most widespread imaging modalities. Hard X-ray tomography (nano computed tomography: nano-CT and micro computed tomography: µCT) is uniquely well suited for investigating soft tissues down to cellular level due to superior penetration power and spatial resolution. AFM: atomic force microscopy (SFM: scanning force microscopy); EM: electron microscopy; LM: light microscopy; OCT: optical coherence tomography; PAT: photoacoustic imaging (optoacoustic imaging); MRI: magnetic resonance imaging; PET: positron-emission tomography.

Currently, *in vivo* clinical imaging modalities, such as computed tomography (CT), magnetic resonance imaging (MRI), positron emission tomography (PET), electroencephalography (EEG), magnetoencephalography (MEG), single-photon emission computed tomography (SPECT) with their functional sub-modalities, such as functional magnetic resonance imaging (fMRI), can only reach a spatial resolution of a fraction of a millimeter, with the exception of specific investigatory sub-modalities, such as microscopic magnetic resonance imaging (µMRI), microscopic positron emission tomography (µPET) and microscopic single photon emission computed tomography (µSPECT), which can reach a micrometer resolution. These techniques are successfully applied for identification of structural and functional changes at the macroscale.[7–9] Moreover, the multi-modal imaging, e.g. PET/CT, SPECT/CT or PET/MRI, combining functional and morphological imaging modalities, has witnessed tremendous progress.

In general, *in vivo* imaging of cells within tissue layers remains a challenge. Many high-resolution microscopy and tomography approaches (photoactivated localisation microscopy (PALM), structured illumination

microscopy (SIM), two-photon fluorescence microscopy (2PFM), optical coherence tomography and microscopy (OCT and OCM), diffuse optical tomography (DOT), photoacoustic tomography (PAT)) offer high sensitivity and resolution for thin and transparent samples, but have a fundamental limit in penetration depth, e.g. due to scattering or attenuation. For example, optical, acoustic or photo-acoustic imaging modalities have a penetration depth of a few millimeters, scanning electron microscopy (SEM) is limited to the surface, and transmission electron microscopy (TEM) to very thin samples. Nevertheless, recent non-invasive, *in vivo*, high-resolution optical methods, such as frequency-domain optical coherence tomography (FDCT) or micro-optical coherence tomography (µOCT),[10] demonstrate the promising results for 3D *in vivo* microscopy[11] with a spatial resolution down to 1 µm. It is believed, that new optical approaches will have a potential to reach depths well beyond what is currently possible.[12] The other powerful *in vivo* imaging modality providing a cellular resolution is stimulated emission depletion (STED) microscopy,[13] one of super-resolution microscopy techniques with can go beyond the diffraction barrier ($\approx$ 240 nm). The modality, however, is limited in penetration depth to micrometer range too.

Until recently, visualising the ultramorphology of human brain tissue has required microscopic examination of stained tissue sections – labour-intensive and time-consuming process as individual sections are mainly handled manually. Light microscopy (LM) remains a gold standard tool in neuroscience for the investigation of brain tissues.[14] However, LM's resolution is limited by a diffraction barrier, thus, subcellular structures are only partially visible. For example, thickness of the cell membrane (plasma membrane, bilayer) is $\sim$ 2 - 10 nm[15,16] – below the resolution limit of light microscopy. Electron microscopy (EM), being the standard technique for the ultrastructural visualisation, has a higher resolving power, i.e. on the nanometer scale and below. The main drawback of the microscopy techniques is the requirement for contrast enhancement. For example, sample preparation for EM includes chemical fixation of the tissue, electron-dense staining and resin embedding, and often specific labelling to identify the structures of interest. In addition to the small sample size, incomplete sampling in microscopy limits tissue context at the organ level.

X-rays are uniquely well suited for investigating ultrastructure of soft tissues, as they are almost unlimited by the penetration depth or wavelength. The wavelengths in the hard X-ray range offer the potential to image at the spatial resolution below a nanometre and the penetration of the hard X-rays through the soft tissues is virtually infinite. Thus, relatively big clinical specimens can be visualised down (sub)cellular level and most of the sample size limitations are related to the technical issues, for example size of the imaging detector, and not to the fundamental limitations. As recently shown, laboratory-based micro computed tomography in the absorption-contrast mode of formalin-fixed paraffin-embedded (FFPE) human cerebellum yields an image contrast comparable to the conventional histological sections.[17] For the 3D visualisation of soft tissues consisting of a low atomic number elements, phase contrast yields a superior data quality compared to the conventional absorption-contrast mode. For example, phase-contrast synchrotron radiation-based double-grating interferometry enabled the identification of non-stained Purkinje cells,[18,19] the synchrotron radiation-based in-line single-distance phase-contrast tomography allowed the automatic quantification of cellular structures with subcellular details.[20]

In this communication, we discuss the preliminary study of brain tissue ultrastructure using synchrotron radiation-based magnified phase-contrast in-line (propagation-based imaging) tomography at the nano-imaging beamline ID16A (European Synchrotron Radiation Facility (ESRF), Grenoble, France) in the single-distance and holotomography (four distances) configurations. As an example, we present images of FFPE human cerebellum block in which structures at the (sub)cellular level are resolved, and labelling was neither used nor required. The results are discussed qualitatively and compared to optical microscopy of haematoxylin and eosin (H&E) stained tissue sections obtained after X-ray based imaging.

Hard X-ray in-line tomography can lead the way in the investigation of the brain ultrastructure in a time-efficient manner. We expect that phase-contrast tomography can provide a valuable information on human tissues in health and disease for many medical applications and basic research, in complementary manner to currently available imaging techniques.

2. MATERIALS AND METHODS

2.1 Specimen preparation

The human cerebellum block was visualised *post mortem*. The brain tissue was extracted from a donated cadaveric body. Written consent for scientific use was documented and all procedures were conducted in accordance

with the Declaration of Helsinki and approved by the Ethikkommission Nordwestschweiz. The cerebellum block was fixed in 4% formalin for a minimum duration of two weeks prior to dissection. Routine sample preparation and paraffin-embedding (plastic polymer mixture Surgipath Paraplast, Leica Biosystems, Switzerland) protocols were applied and have been carried out in a diagnostic neuropathology laboratory without modification.[17,20] A cylinder 1.6 mm in height was extracted from the standard histological paraffin block using a metal punch with an inner diameter of 510 µm.

2.2 Laboratory-based absorption-contrast micro computed tomography

The cylindrical specimen was preliminary evaluated by means of laboratory-based absorption-contrast micro computed tomography by the commercially available system nanotom® m (GE Sensing & Inspection Technologies GmbH, Wunstorf, Germany) equipped with a 180 kV/15 W nanofocus® transmission tube with an adjustable focal spot diameter and operated with a tungsten target.[21] The focal spot diameter was adjusted to $w = 1$ µm. The laboratory-based tomography was performed in the *fast scan*® mode with a total scan time of 12 minutes, an effective pixel size 1 µm, a tube voltage of 60 kVp, and a beam current of 350 µA. Data processing and reconstruction were done automated, using the datos|x 2.0 software (phoenix|x-ray, GE Sensing & Inspection Technologies GmbH, Wunstorf, Germany).

2.3 Nano-holotomography

Figure 2 shows the schema (Fig. 2A) and photographs (Fig. 2B, B1, B2) of the experimental set-up used for synchrotron radiation-based hard X-ray magnified phase-contrast in-line tomography. The tomography imaging experiments were performed at the nano-imaging beamline ID16A (ESRF, Grenoble, France)[22] in the single-distance (one focus-sample distance d_0) and holotomography (four focus-sample distances d_1 - d_4) configurations. The synchrotron radiation is monochromatised and focused by X-ray reflective optics (multilayer-coated mirrors - Kirkpatrick-Baez[23] crossed mirror geometry). The sample is moved down from the pre-vacuum chamber (Fig. 2B1), positioned on a translation-rotation stage in the vacuum chamber (Fig. 2B2) with the pressure between 10^{-7} and 10^{-8} mbar, and imaged onto a stationary detector. Due to the cone-beam geometry, four pre-selected focus-sample distances (d_1, d_2, d_3, d_4) used for the holotomography and one (d_0) for the single-distance tomography imply related magnification factors on the detector, resulting in the effective pixel sizes.

As the sample was larger ($d_\varnothing = 510$ µm) than the field of view (FOV), local tomography measurements were performed. An X-ray energy of 17 keV was selected. The experimental parameters are summarised in Table 1. The retrieved phase maps[24,25] were input to a tomographic reconstruction algorithm based on filtered back-projection algorithm[26] using PyHST2. The technical details of the imaging set-up have been described previously.[22]

Table 1. Scanning parameters. All scans were performed at a photon energy of 17 keV. l: effective pixel size; N: number of projections; t: exposure time; d: the focus to sample distances.

Scan number	**Tissue**	$\boldsymbol{l}$ [nm]	$\boldsymbol{N}$	$\boldsymbol{t}$ [s]	$\boldsymbol{d}$ [mm]
1	FFPE Cerebellum	200	1200	0.3	80.533
2	FFPE Cerebellum	100	1900	0.3	40.266, 41.994, 48.904, 63.251

2.4 Histology

Subsequent to the tomography, the paraffin cylinder containing the tissue was re-embedded in a standard histological paraffin block, sectioned, stained and visualised by optical microscopy. Sections of 4 µm thickness were cut using a microtome, mounted on glass slides, and stained with H&E following the standard protocols without modification.[17,20] Images of the resulting slides were taken on a light microscope and resulted in the pixel sizes of 6.99 µm and 4.38 µm (optical magnifications 10× and 40×), respectively.[17]

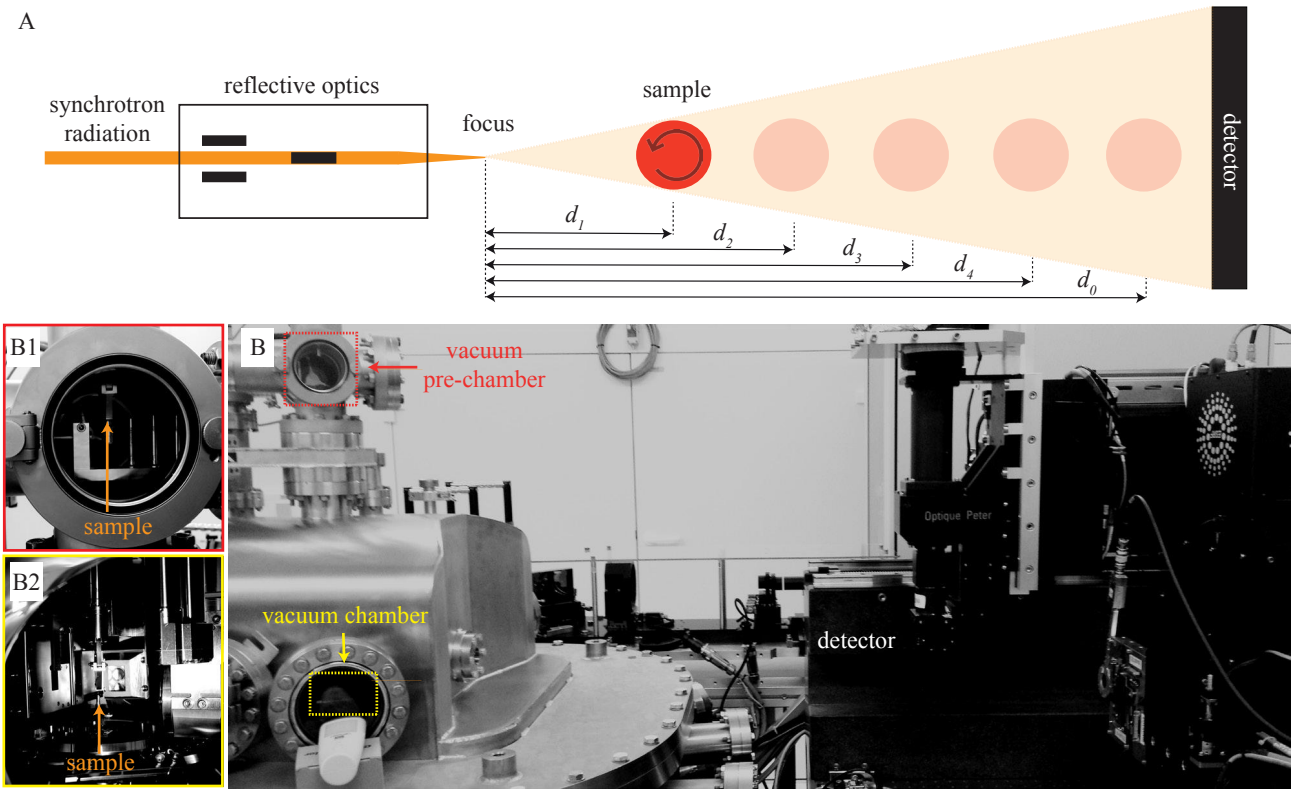

Figure 2. Schema (A) and photographs (B, B1, B2) of the experimental setup for single-distance tomography and holotomography. The synchrotron radiation is monochromatised and focused by X-ray reflective optics. The sample is moved down from the pre-vacuum chamber (B1), positioned on a translation-rotation stage in the vacuum chamber (B2) and imaged onto a stationary detector. Due to the cone-beam geometry, four pre-selected focus-sample distances (d_1, d_2, d_3, d_4) used for the holotomography and one (d_0) for the single-distance tomography imply different magnification factors on the detector.

2.5 Data registration

To locate the counterpart of histology in the tomography volume, expert-based registration was performed in MATLAB® (2016a, The MathWorks, Inc., Natick, Massachusetts, USA).[17,27]

Datasets acquired in the single-distance and holotomography configurations were registered using an automated 3D/3D registration tool[28–30] with rigid transformation constraints. The dataset acquired in the single-distance configuration was used as reference.

3. RESULTS AND DISCUSSION

3.1 Imaging workflow

The conventional approach for visualising soft tissues with a (sub)cellular resolution within a clinical environment remains optical microscopy of stained tissue sections.[31,32] The specimen preparation for the optical microscopy is a multi-step process which includes extraction of the tissues from a patient or donated body, chemical fixation to preserve from decay, serial dehydration, paraffin embedding, sectioning, and staining, as represented by the scheme in Figure 3. Apart from possible slicing or staining artifacts, this methodology is time-consuming, making it almost impossible to cover the complete 3D microarchitecture[29,33,34] of a relatively large tissue specimen. In addition, this methodology is destructive[32] and the spatial resolution in one direction is limited by the section thickness to the micrometer range. Moreover, the cut direction can only partially be controlled and has a fundamental limitations, for example due to the maximal possible tilting angle. Nevertheless, Purkinje cells, a population of large cerbellar neurons, have been successfully resolved down to subcellular structures using

wide range of techniques: light microscopy, transmission electron microscopy, scanning electron microscopy, freeze etching techniques, field emission scanning electron microscopy, cryofracture methods, and confocal laser scanning microscopy.[35]

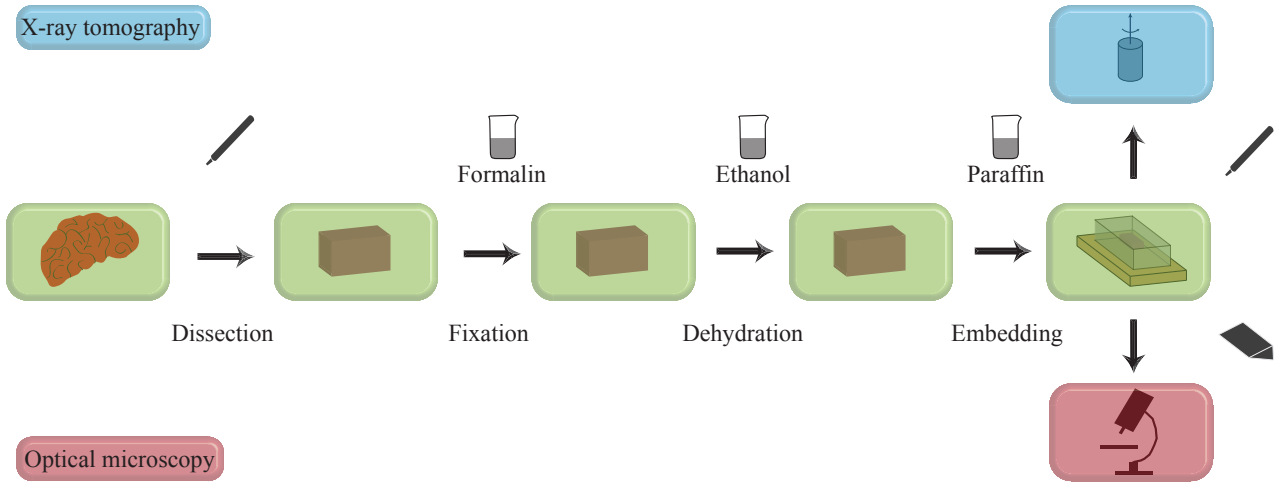

Figure 3. Imaging workflow: Schematic representation of the specimen preparation procedures for the optical microscopy examination and X-ray tomography, including dehydration and paraffin embedding according to surgical pathology procedures.

At the same time, X-ray imaging modalities can offer a (sub)cellular resolution for the large tissue volumes in a non-destructive and time-efficient manner[20,36–39] where the same FFPE sample prepared for the histological examination can be used (Figure 3). In the case of tomography, specimen preparation is less expensive. This tomographic approach is, therefore, complementary and may help to select the cutting plane for histological sectioning.[27]

X-ray tomography with the nanoscale resolution is of a great interest for many applications in the life sciences.[40] Most of the synchrotron radiation facilities worldwide, based on the parallel-beam geometry, have intrinsic limitations in the spatial resolution to a few hundreds of nanometers, for example, due to detector specifications.[41] To overcome these limitations, and reach a sub-100-nm resolution, cone-beam geometry can be used.[41] Synchrotron radiation-based phase-contrast X-ray in-line tomography[25,42,43] is a powerful imaging modality that do not require the use of optical elements between the sample and detector (in contrast to, e.g., grating interferometry[18,19]) and has the advantage of simplicity and increased resolution. In case of in-line tomography, the spatial resolution is not limited by the reflective optics, so the improvement of the spatial resolution from a fraction of a micrometre to a few nanometers is foreseen.[44]

3.2 Comparison of tomography and light microscopy-based imaging

To demonstrate the performance of the in-line phase-contrast tomography for brain imaging with nanoscale spatial resolution, we scanned FFPE human cerebellum specimen with an effective pixel size of 200 nm in the single-distance configuration by means of synchrotron radiation-based magnified phase-contrast in-line tomography at the nano-imaging beamline ID16A. Optical microscopy of H&E-stained histological sections was the method we chose to validate the tomography imaging results. Figure 4 shows a comparison between H&E-stained histological sections (optical magnification 10×) (Fig. 4 A, C) and single-distance tomography slices (Fig. 4 B, D). Magnifications into the registered data (Fig. 4 E-H) show that tomography and histology (optical magnification 40×) can provide similar information. Both modalities can resolve individual Purkinje, granule and stellate cells within the human cerebellum specimen. In general, 2D/3D registration of individual histological sections with a large 3D tomography data is a challenge.[45] Nevertheless, it is essential correlating tomography observations with the gold standard histology.

Figure 4 I shows combined image of the individual Purkinje cell visualised by means of optical microscopy (left) and single-distance tomography (right). Both modalities can resolve the cell soma, some inner content

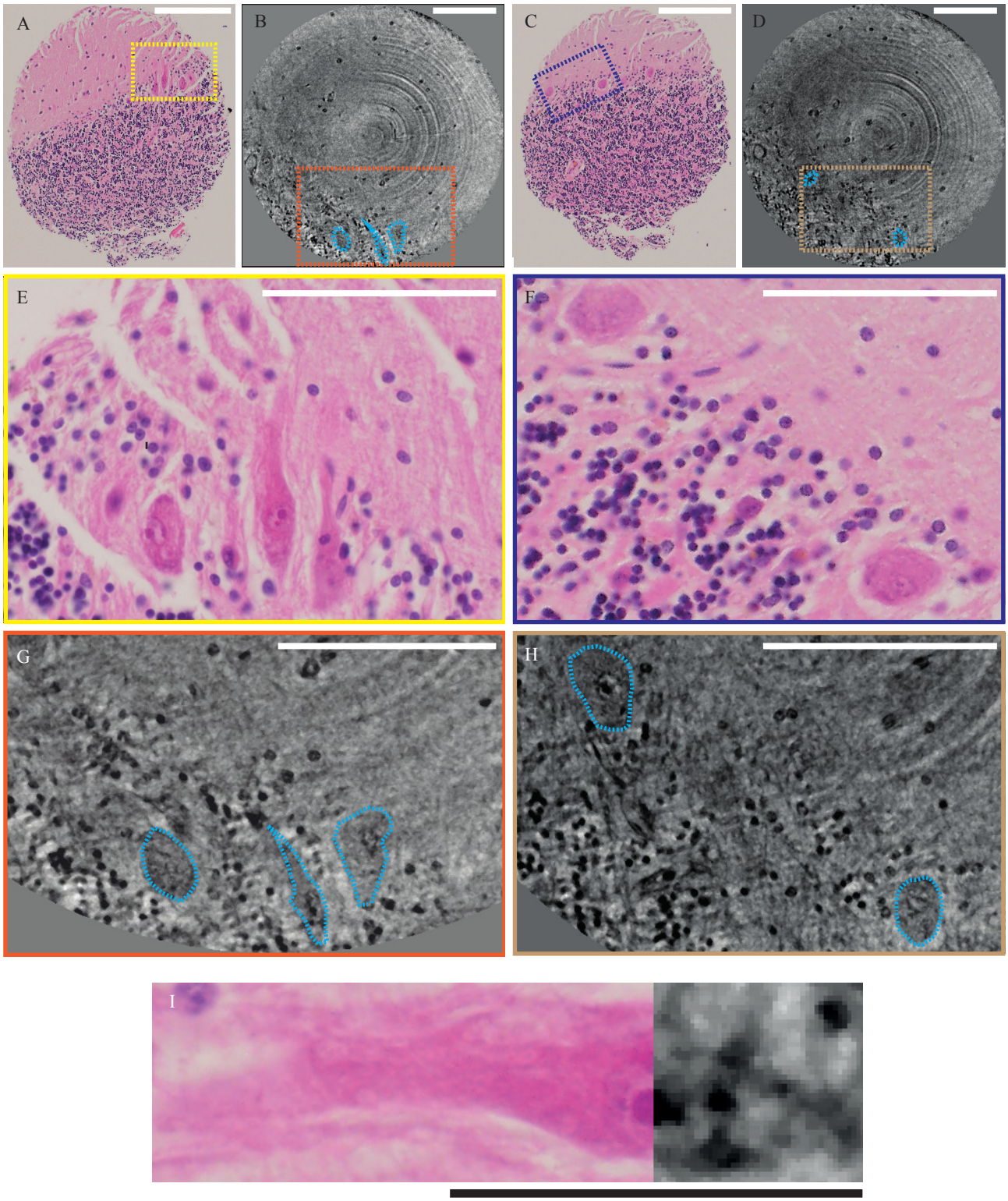

Figure 4. Qualitative comparison of the H&E-stained histological sections (A, C) and single-distance tomography slices (B, D) on the example of FFPE human cerebellum block. Magnifications (E, F) into the manually pre-registered histological sections highlight similarity to the tomography data (G, H). Combined image (I) showcase the complementarity of the data. Blue dashed line: Purkinje cells. White scale bars correspond to 100 µm. Black scale bar corresponds to 50 µm.

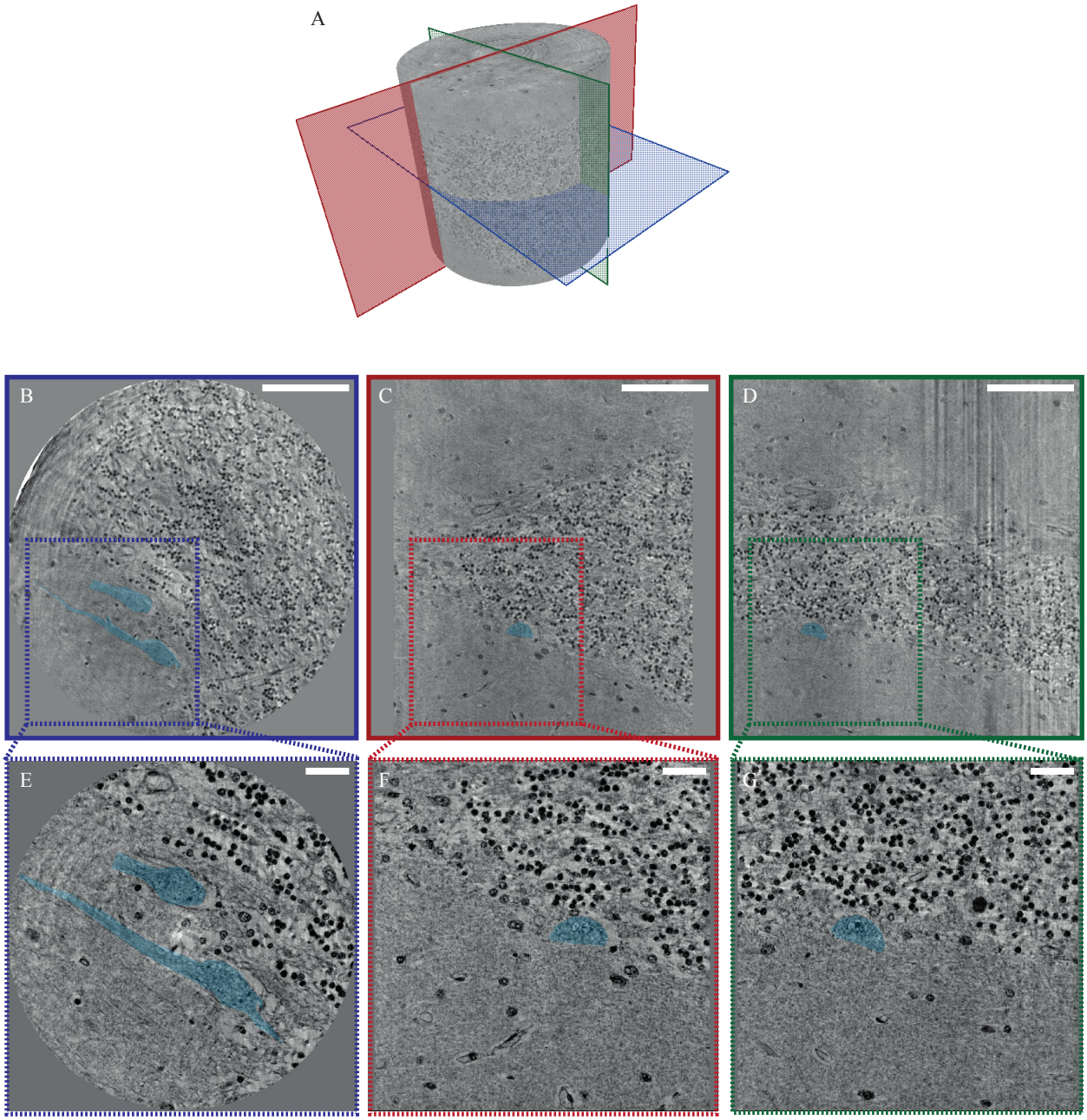

Figure 5. Based on the single-distance prescan (A - D) the region of interest can be selected and hierarchically imaged with an increasing magnification in the holotomography configuration, for example with an effective pixel size of 100 nm (E - G). Virtual cross-sections through the FFPE cerebellum block: transverse (B, E), frontal (C, F) and sagittal (D, G) view. Blue: Purkinje cells.Scale bars correspond to 100 µm.

of the plasma membrane, nucleus, nucleolus, nuclear envelope, dendritic and axonal processes. The advantage of tomography is that (sub)cellular structures can be analyses in a three-dimensional view, in contrast to microscopy.[35]

Already in the single-distance configuration, in-line tomography provides information well comparable to histology. The further effective pixel decrease can enhance the in-line tomography in ultrastructural imaging, potentially, useful for understanding brain disorders. Purkinje, granule and stellate cells identified by single-distance tomography can be further characterised by the use of a higher magnification imaging data acquired in the holotomography configuration. As a proof-of-concept demonstrated, imaging data was recorded with effective pixel sizes of 200 nm (Fig. 5 A-D) in the single-distance configuration and 100 nm (Fig. 5 E-G) in the holotomography configuration. After 3D/3D registration, the higher resolution data can be precisely localised within the lower resolution ones.

4. CONCLUSION AND OUTLOOK

Nowadays, nanoimaging of human tissues is extremely popular topic of research. Due to the nanometer resolution, reasonable specimen preparation, and large penetration depth, tomography is a promising tool for imaging the ultrastructure of selected brain tissues *post mortem*. Moreover, this effective imaging technique can be extended to other soft tissues.

Holotomographic imaging offers excellent spatial resolution, but requires a relatively long acquisition times – 4× the time required for the single-distance imaging. Thus, single-distance phase-contrast tomography can become a method of choice for time-efficient investigations.

For the investigations of brain tissues down to the subcellular level microscopy techniques, such as EM or LM, have already proven their applicability, and relevant computational approaches have been developed and successfully applied, for example, approaches for correlating LM and EM[46] or data segmentation.[47,48] Nevertheless, the approaches to extract the neural network automatically are still a subject to research and belong to an unsolved problems. Similar computational approaches can be developed or adapted for in-line tomography in future.

Synchrotron radiation-based magnified phase-contrast in-line tomography of FFPE brain tissues is currently in the early stage of development, offering both a challenge and an opportunity. First, we have noted that FFPE tissue blocks can crack after the vacuum environment making it complex to perform further histopathological investigations, although it does not influence nanoscopic observations of the tomography itself. Other potential tissue artifacts are minimal. It also remains to be determined how accessible different classes of biological information from FFPE tissue may be.

The authors expect that in-line tomography will become a complementary method to enhance histology.

5. ACKNOWLEDGEMENTS

The authors acknowledge the financial support of the Swiss National Science Foundation (SNSF) projects 147172, 150164, 147172, and SNSF R'Equip project 133802. The project was supported by the ESRF proposal MD-969.

REFERENCES

[1] Chung, K. and Deisseroth, K., "CLARITY for mapping the nervous system," *Nat. Methods.* **10**(6), 508–513 (2013).

[2] Amunts, K., Lepage, C., Borgeat, L., Mohlberg, H., Dickscheid, T., Rousseau, M.-E., Bludau, S., Bazin, P.-L., Lewis, L., Oros-Peusquens, A.-M., Shah, N., Lippert, T., Zilles, K., and Evans, A., "BigBrain: An ultrahigh-resolution 3D human brain model," *Science* **340**(6139), 1472–1475 (2013).

[3] Olesen, J. and Leonardi, M., "The burden of brain diseases in europe," *Eur. J. Neurol.* **10**(5), 471–477 (2003).

[4] Petersen, C., "The functional organization of the barrel cortex," *Neuron* **56**(2), 339–355 (2007).

[5] Mombaerts, P., Wang, F., Dulac, C., Chao, S., Nemes, A., Mendelsohn, M., Edmondson, J., and Axel, R., "Visualizing an olfactory sensory map," *Cell* **87**(4), 675–686 (1996).

[6] Pfister, H., Kaynig, V., Botha, C., Bruckner, S., Dercksen, V., Hege, H.-C., and Roerdink, J., "Visualization in connectomics," *Math. Vis.* **37**, 221–245 (2014).

[7] Stefanescu, M., Dohnalek, M., Maderwald, S., Thürling, M., Minnerop, M., Beck, A., Schlamann, M., Diedrichsen, J., Ladd, M., and Timmann, D., "Structural and functional MRI abnormalities of cerebellar cortex and nuclei in SCA3, SCA6 and Friedreich's ataxia," *Brain* **138**(5), 1182–1197 (2015).

[8] Law, N., Greenberg, M., Bouffet, E., Laughlin, S., Taylor, M., Malkin, D., Liu, F., Moxon-Emre, I., Scantlebury, N., Skocic, J., and Mabbott, D., "Visualization and segmentation of reciprocal cerebrocerebellar pathways in the healthy and injured brain," *Hum. Brain Mapp.* **36**(7), 2615–2628 (2015).

[9] Kim, J., Shin, J., Oh, J.-H., Jung, H., Kim, Y.-B., Cho, Z.-H., and Chang, J., "Longitudinal FDG microPET imaging of neuropathic pain: does cerebellar activity correlate with neuropathic pain development in a rat model?," *Acta Neurochir.* **157**(6), 1051–1057 (2015).

[10] Liu, L., Gardecki, J., Nadkarni, S., Toussaint, J., Yagi, Y., Bouma, B., and Tearney, G., "Imaging the subcellular structure of human coronary atherosclerosis using micro-optical coherence tomography," *Nat. Med.* **17**(8), 1010–1014 (2011).

[11] Yoo, H., Kim, J., Shishkov, M., Namati, E., Morse, T., Shubochkin, R., McCarthy, J., Ntziachristos, V., Bouma, B., Jaffer, F., and Tearney, G., "Intra-arterial catheter for simultaneous microstructural and molecular imaging in vivo," *Nat. Med.* **17**(12), 1680–1684 (2011).

[12] Gigan, S., "Optical microscopy aims deep," *Nat. Photonics* **11**(1), 14–16 (2017).

[13] Berning, S., Willig, K., Steffens, H., Dibaj, P., and Hell, S., "Nanoscopy in a living mouse brain," *Science* **335**(6068), 551 (2012).

[14] Choe, A., Gao, Y., Li, X., Compton, K., Stepniewska, I., and Anderson, A., "Accuracy of image registration between MRI and light microscopy in the ex vivo brain," *J. Magn. Reson. Imaging* **29**(5), 683–692 (2011).

[15] Cell biology by the numbers, "What is the thickness of the cell membrane?," *available online at: http://book.bionumbers.org/what-is-the-thickness-of-the-cell-membrane/* (06.08.2017).

[16] The Physics Factbook: An encyclopedia of scientific essays, "Thickness of a cell membrane," *available online at: https://hypertextbook.com/facts/2001/JenniferShloming.shtml* (06.08.2017).

[17] Khimchenko, A., Deyhle, H., Schulz, G., Schweighauser, G., Hench, J., Chicherova, N., Bikis, C., Hieber, S., and Müller, B., "Extending two-dimensional histology into the third dimension through conventional micro computed tomography," *NeuroImage* **139**, 26–36 (2016).

[18] Schulz, G., Weitkamp, T., Zanette, I., Pfeiffer, F., Beckmann, F., David, C., Rutishauser, S., Reznikova, E., and Müller, B., "High-resolution tomographic imaging of a human cerebellum: Comparison of absorption and grating-based phase contrast," *J. R. Soc. Interface* **7**(53), 1665–1676 (2010).

[19] Schulz, G., Weitkamp, T., Zanette, I., Pfeiffer, F., Müller-Gerbl, M., David, C., and Müller, B., "Asymmetric rotational axis reconstruction of grating-based X-ray phase contrast tomography of the human cerebellum," *Proc. SPIE* **8506**, 850604 (2012).

[20] Hieber, S. E., Bikis, C., Khimchenko, A., Schweighauser, G., Hench, J., Chicherova, N., Schulz, G., and Müller, B., "Tomographic brain imaging with nucleolar detail and automatic cell counting," *Sci. Rep.* **6**, 32156 (2016).

[21] Egbert, A. and Brunke, O., "High-resolution X-ray computed tomography for materials research," *Adv. Mat. Res.* **222**, 48–51 (2011).

[22] European Synchrotron Radiation Facility (ESRF), "ID16A - Nano-imaging Beamline," *available online at: http://www.esrf.eu/UsersAndScience/Experiments/XNP/ID16A* (02.08.2017).

[23] Kirkpatrick, P. and Baez, A., "Formation of optical images by x-rays," *J. Opt. Soc. Am.* **38**(9), 766–774 (1948).

[24] Bleuet, P., Cloetens, P., Gergaud, P., Mariolle, D., Chevalier, N., Tucoulou, R., Susini, J., and Chabli, A., "A hard x-ray nanoprobe for scanning and projection nanotomography," *Rev. Sci. Instrum.* **80**(5), 056101 (2009).

[25] Cloetens, P., Ludwig, W., Baruchel, J., Van Dyck, D., Van Landuyt, J., Guigay, J. P., and Schlenker, M., "Holotomography: Quantitative phase tomography with micrometer resolution using hard synchrotron radiation x rays," *Appl. Phys. Lett.* **75**(19), 2912–2914 (1999).

[26] Mirone, A., Brun, E., Gouillart, E., Tafforeau, P., and Kieffer, J., "The PyHST2 hybrid distributed code for high speed tomographic reconstruction with iterative reconstruction and a priori knowledge capabilities," *Nucl. Instrum. Methods Phys. Res. B* **324**, 41–48 (2014).

[27] Stalder, A., Ilgenstein, B., Chicherova, N., Deyhle, H., Beckmann, F., Müller, B., and Hieber, S., "Combined use of micro computed tomography and histology to evaluate the regenerative capacity of bone grafting materials," *Int. J. Mat. Res.* **105**(7), 679–691 (2014).

[28] Andronache, A., von Siebenthal, M., Székely, G., and Cattin, P., "Non-rigid registration of multi-modal images using both mutual information and cross-correlation," *Med. Image Anal.* **12**(1), 3–15 (2008).

[29] Müller, B., Deyhle, H., Lang, S., Schulz, G., Bormann, T., Fierz, F., and Hieber, S., "Three-dimensional registration of tomography data for quantification in biomaterials science," *Int. J. Mater. Res.* **103**(2), 242–249 (2012).

[30] Buscema, M., Schulz, G., Deyhle, H., Khimchenko, A., Matviykiv, S., Holme, M., Hipp, A., Beckmann, F., Saxer, T., Michaud, K., and Müller, B., "Histology-validated X-ray tomography for imaging human coronary arteries," *Proc. SPIE* **9967**, 99670O (2016).

[31] Krenkel, M., Markus, A., Bartels, M., Dullin, C., Alves, F., and Salditt, T., "Phase-contrast zoom tomography reveals precise locations of macrophages in mouse lungs," *Sci. Rep.* **5**, 9973 (2015).

[32] Lang, S., Zanette, I., Dominietto, M., Langer, M., Rack, A., Schulz, G., Le Duc, G., David, C., Mohr, J., Pfeiffer, F., Müller, B., and Weitkamp, T., "Experimental comparison of grating- and propagation-based hard X-ray phase tomography of soft tissue," *J. Appl. Phys.* **116**(15), 154903 (2014).

[33] Schulz, G., Morel, A., Imholz, M., Deyhle, H., Weitkamp, T., Zanette, I., Pfeiffer, F., David, C., Müller-Gerbl, M., and Müller, B., "Evaluating the microstructure of human brain tissues using synchrotron radiation-based micro computed tomography," *Proc. SPIE* **7804**, 78040F (2010).

[34] Germann, M., Morel, A., Beckmann, F., Andronache, A., Jeanmonod, D., and Müller, B., "Strain fields in histological slices of brain tissue determined by synchrotron radiation-based micro computed tomography," *J. Neurosci. Meth.* **170**(1), 149–155 (2008).

[35] Castejón, O. J., "Review: Correlative microscopy of Purkinje cells," *Biocell* **35**(3), 1–29 (2011).

[36] Zehbe, R., Haibel, A., Riesemeier, H., Gross, U., Kirkpatrick, C., Schubert, H., and Brochhausen, C., "Going beyond histology. Synchrotron micro-computed tomography as a methodology for biological tissue characterization: From tissue morphology to individual cells," *J. R. Soc. Interface* **7**(42), 49–59 (2010).

[37] Huang, S., Kou, B., Chi, Y., Xi, Y., Cao, Y., Cui, W., Hu, X., Shao, Z., Guo, H., Fu, Y., Xiao, T., Sun, J., Zhao, J., Wang, Y., and Wu, J., "In-line phase-contrast and grating-based phase-contrast synchrotron imaging study of brain micrometastasis of breast cancer," *Sci. Rep.* **5**, 9418 (2015).

[38] Zehbe, R., Schmitt, V. H., Kirkpatrick, C. J., and Brochhausen, C., "High resolution X-ray tomography - Three-dimensional characterisation of cell-scaffold constructs for cartilage tissue engineering," *Mater. Sci. Tech. (UK)* **31**(2), 167–173 (2015).

[39] Langer, M., Pacureanu, A., Suhonen, H., Grimal, Q., Cloetens, P., and Peyrin, F., "X-ray phase nanotomography resolves the 3D human bone ultrastructure," *PLoS ONE* **7**, 8 (2012).

[40] Sakdinawat, A. and Attwood, D., "Nanoscale x-ray imaging," *Nat. Photon.* **4**(12), 840–848 (2010).

[41] Stampanoni, M., Mokso, R., Marone, F., Vila-Comamala, J., Gorelick, S., Trtik, P., Jefimovs, K., and David, C., "Phase-contrast tomography at the nanoscale using hard X-rays," *Phys. Rev. B* **81**(14), 140105 (2010).

[42] Cloetens, P., Barrett, R., Baruchel, J., Guigay, J.-P., and Schlenker, M., "Phase objects in synchrotron radiation hard x-ray imaging," *J. Phys. D: Appl. Phys.* **29**(1), 133–146 (1996).

[43] Zanette, I., Lang, S., Rack, A., Dominietto, M., Langer, M., Pfeiffer, F., Weitkamp, T., and Müller, B., "Holotomography versus x-ray grating interferometry: A comparative study," *Applied Physics Letters* **103**(24), 244105 (2013).

[44] Mimura, H., Handa, S., Kimura, T., Yumoto, H., Yamakawa, D., Yokoyama, H., Matsuyama, S., Inagaki, K., Yamamura, K., Sano, Y., Tamasaku, K., Nishino, Y., Yabashi, M., Ishikawa, T., and Yamauchi, K., "Breaking the 10 nm barrier in hard-x-ray focusing," *Nat. Phys.* **6**(2), 122–125 (2010).

[45] Chicherova, N., Hieber, S., Schulz, G., Khimchenko, A., Bikis, C., Cattin, P., and Müller, B., "Automatic histology registration in application to X-ray modalities," *Proc. SPIE* **9967**, 996708 (2016).

[46] Shu, X., Lev-Ram, V., Deerinck, T., Qi, Y., Ramko, E., Davidson, M., Jin, Y., Ellisman, M., and Tsien, R., "A genetically encoded tag for correlated light and electron microscopy of intact cells, tissues, and organisms," *PLoS Biol.* **9**(4) (2011).

[47] Kreshuk, A., Straehle, C., Sommer, C., Koethe, U., Cantoni, M., Knott, G., and Hamprecht, F., "Automated detection and segmentation of synaptic contacts in nearly isotropic serial electron microscopy images," *PLoS ONE* **6**(10) (2011).

[48] Straehle, C., Köthe, U., Knott, G., and Hamprecht, F., "Carving: scalable interactive segmentation of neural volume electron microscopy images," *Lect. Notes in Comput. Sci.* **14**(1), 653–660 (2011).